FRONTIERS OF PHYSICS

RESEARCH ARTICLE
Volume 19 / Issue 5 / 51205 / 2024

Hardware-efficient and fast three-qubit gate in superconducting quantum circuits

Xiao-Le Li[1,2,*], Ziyu Tao[2,3,*], Kangyuan Yi[2,3], Kai Luo[2,3], Libo Zhang[3,4], Yuxuan Zhou[2,3], Song Liu[3,4,5], Tongxing Yan[3,4,5,†], Yuanzhen Chen[2,3,5,‡], Dapeng Yu[2,3,4,5]

1 Department of Physics, Harbin Institute of Technology, Harbin 150001, China
2 Department of Physics, Southern University of Science and Technology, Shenzhen 518055, China
3 Shenzhen Institute for Quantum Science and Engineering, Southern University of Science and Technology, Shenzhen 518055, China
4 Shenzhen International Quantum Academy (SIQA), Shenzhen 518048, China
5 Guangdong Provincial Key Laboratory of Quantum Science and Engineering, Southern University of Science and Technology, Shenzhen 518055, China
*These authors contributed equally to this work.
Corresponding authors. E-mail: †yantx@sustech.edu.cn, ‡chenyz@sustech.edu.cn
Received February 17, 2024; accepted March 25, 2024

ABSTRACT

While the common practice of decomposing general quantum algorithms into a collection of single- and two-qubit gates is conceptually simple, in many cases it is possible to have more efficient solutions where quantum gates engaging multiple qubits are used. In the noisy intermediate-scale quantum (NISQ) era where a universal error correction is still unavailable, this strategy is particularly appealing since it can significantly reduce the computational resources required for executing quantum algorithms. In this work, we experimentally investigate a three-qubit Controlled-CPHASE-SWAP (CCZS) gate on superconducting quantum circuits. By exploiting the higher energy levels of superconducting qubits, we are able to realize a Fredkin-like CCZS gate with a duration of 40 ns, which is comparable to typical single- and two-qubit gates realized on the same platform. By performing quantum process tomography for the two target qubits, we obtain a process fidelity of 86.0% and 81.1% for the control qubit being prepared in $|0\rangle$ and $|1\rangle$, respectively. We also show that our scheme can be readily extended to realize a general CCZS gate with an arbitrary swap angle. The results reported here provide valuable additions to the toolbox for achieving large-scale hardware-efficient quantum circuits.

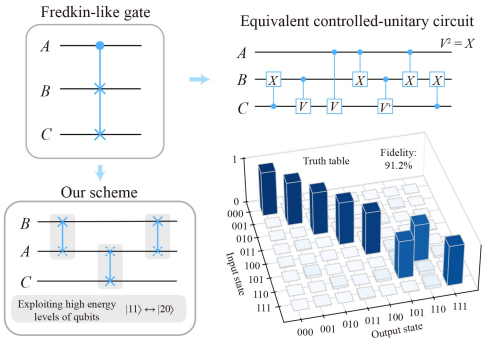

Keywords quantum computation, quantum gate, superconducting circuit

In realistic quantum circuits, errors may occur in different forms including, for example, stochastic errors resulting from decoherence and coherent errors due to control imperfections. While remarkable progress of quantum error correction has been achieved in recent years [1–3], a fault-tolerant universal quantum computer is still far beyond the reach of today's technology of quantum information processing (QIP). It has been widely believed that in a rather long period from now, we will be in the NISQ era [4–6]. To combat the various

Higher Education Press

https://doi.org/10.1007/s11467-024-1405-8

types of errors mentioned above in the NISQ era, one top priority is to develop hardware-efficient implementations of quantum algorithms, which aims at minimizing the impact of errors by reducing the spatiotemporal complexity of quantum circuits.

Multi-qubit quantum gates, such as the Fredkin (controlled-SWAP) and Toffoli (and its equivalent controlled-controlled-Z) gates, are widely used in quantum information processing for this purpose. For instance, using such gates helps reduce the circuit depth for variational quantum eigensolver [7–9]. Moreover, these gates can simulate effective many-body interaction, which appears in a variety of proposals of quantum simulations [10–12]. A common practice of implementing such multi-qubit gates is to decompose them into a collection of standard single- and two-qubit gates. However, when complied this way, it takes eight (six) CNOT (controlled-NOT) gates to realize a Fredkin (Toffoli) gate in addition to several single-qubit gates, even for the case of an all-to-all connectivity [13]. Therefore finding more efficient ways of implementing such multi-qubit gates are highly desirable.

Thus far, Toffoli gate has been extensively investigated on various platforms [14–17]. In superconducting quantum circuits, the performance of Toffoli gate has been significantly improved recently [18–23]. On the contrary, the Fredkin gate has been less explored experimentally, even though several protocols were proposed [24–27]. Warren *et al.* [22] implemented a family of three-qubit gates (including the Fredkin gate) based on simultaneous two-qubit operations in superconducting circuits. However, the weak interaction in their work resulted in a long gate duration. Furthermore, simultaneously turning on the interaction may complicate the tuning up process.

In this work, we report an experimental realization of a Fredkin-like Controlled-CPHASE-SWAP (CCZS) gate [19, 22] that inverts the states of two target qubits and realizes a conditional phase operation, upon the state of the third qubit. Following the common practice, we also decompose such a three-qubit gate into a sequence of single- and two-qubit gates. However, by exploiting the higher energy levels of the qubits, we are able to shorten the duration of a three-qubit Fredkin gate to around 40 ns, which is comparable to the durations of typical single- and two-qubit gates widely used in superconducting quantum computation. We characterize this gate by measuring its truth table and performing quantum process tomography for the two target qubits when the control qubit is prepared in $|0\rangle$ and $|1\rangle$, and obtain a truth table fidelity of 91.2% and a process fidelity of $\mathrm{Tr}(\chi^0_{\mathrm{exp}}\chi^0_{\mathrm{ideal}}) = 86.0\%$, $\mathrm{Tr}(\chi^1_{\mathrm{exp}}\chi^1_{\mathrm{ideal}}) = 81.1\%$. The dominant errors are due to decoherence and distortion in signals controlling qubits' frequencies. The signal distortion induces an incomplete swap between $|11\rangle$ and $|20\rangle$ and thus affects the gate operation. Using the above three-qubit operation, we demonstrate fast generation of a GHZ state with a fidelity of 96.5%, suggesting its promising applications in QIP.

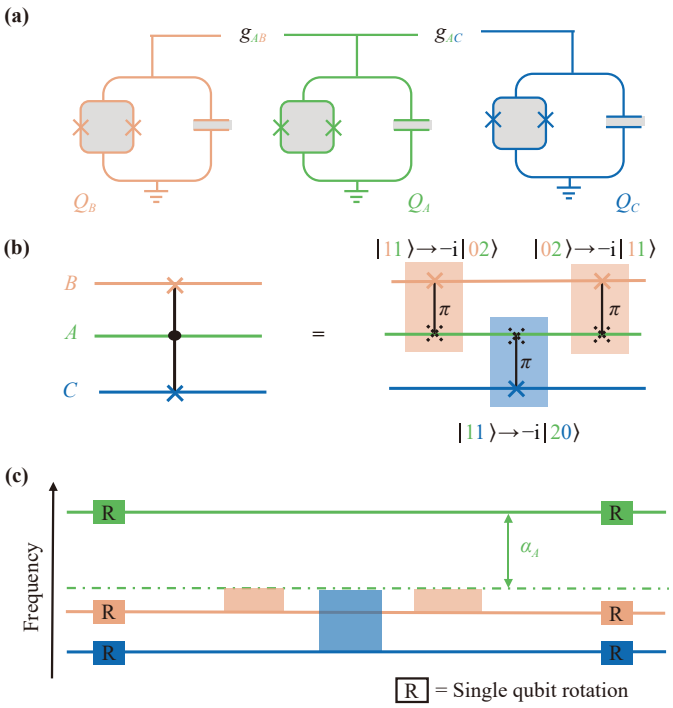

Fig. 1 Schematics of the superconducting qubits and circuit diagram used in this work for a Controlled-CPHASE-SWAP (CCZS) gate. **(a)** Sketch of the device with three transmon qubits of tunable frequencies. Eeach qubit contains a SQUID (superconducting quantum interference device) ring whose magnetic flux can be varied by a current flowing on a on-chip flux line nearby (not shown), which in turn changes the qubit's frequency. Each qubit is equipped with its own flux line, control line, and readout resonator (not shown) as widely used in the transmon-based superconducting quantum circuits. Adjacent qubits are coupled and share a common feedline for dispersive readout. **(b)** Schematics of our scheme decomposing a Fredkin-like CCZS gate into a sequence of three iSWAP operations (marked as ×) between adjacent qubits. Each iSWAP operation represents a coherent π rotation realized by tuning the $|11\rangle$ state of the involved two qubits into resonance with the $|20\rangle$ state. The overall operation is then a Fredkin-like CCZS gate: a controlled-iSWAP operation between two target qubits Q_B and Q_C upon the status of the control qubit Q_A. If Q_A is in its excited states $(\cdot)$, an controlled-iSWAP occurs between Q_B and Q_C. **(c)** Pulse sequence for benchmarking the CCZS gate. Single-qubit gates, marked as R, are used for preparing different initial states and rotating the three-qubit state for projection measurements.

The experiment is carried out in a superconducting quantum circuit that consists of three frequency-tunable superconducting transmon qubits, as sketched in Fig. 1(a). The three transmon qubits [28] are labelled as $Q_{A,B,C}$. In this work, Q_A serves as the control qubit for all the three-qubit operations. The anharmonicity for the three qubits is around $\alpha_{A,B,C}/(2\pi) = -0.19$ GHz, and their idling frequencies are $\omega^A_{10}/(2\pi) = 4.308$ GHz,

$\omega_{10}^{B}/(2\pi)$ =4.068 GHz, and $\omega_{10}^{C}/(2\pi) = 4.084$ GHz. The nearest neighbouring qubits are effectively coupled via a tunable coupler [29], and the working coupling strengths are $g_{AB}^{10,01}/(2\pi)$ =$g_{AC}^{10,01}/(2\pi) = 14.2$ MHz , which is benchmarked by tuning two adjacent qubits into resonance and measuring the rate of their iSWAP operation. Throughout this work, we use the upper index of ij, kl to explicitly indicate the two basis states involved in the exchange. Each qubit has its own individual control line for microwave pulses of single-qubit operations and individual flux line for varying its frequency. Moreover, each qubit is equipped with a dedicated resonator for dispersive readout, and all three readout resonators share a common feedline. We use the ground and first excited states of each qubit as the computational basis $|0\rangle$ and $|1\rangle$. The second excited state $|2\rangle$ serves as an ancilla for realizing the three-qubit gate operations. At the idling frequencies, the relaxation time T_1^{10} of the first excited state is characterized to be 33.7 μs, 21.6 μs, and 27.2 μs, respectively, for the three qubits. The dephasing time T_2^{10} benchmarked by the standard Ramsey experiment is 1.3 μs, 2.8 μs, and 2.5 μs for the three qubits, respectively.

As mentioned above, we implement the CCZS gate by decomposing it into a sequence of single- and two-qubit gates. Here the essential components are several iSWAP operations between adjacent qubits. In the following we first discuss such iSWAP operations. For example, let us consider qubits Q_A and Q_B. If their first excited states are tuned into resonance, that is, the condition $f_{10}^{A} = f_{10}^{B}$ is satisfied, an exchange of energy between the qubits occurs at a rate of $2g_{AB}^{10,01}$. An iSWAP gate between the two basis states of $|10\rangle$ and $|01\rangle$ can thus be accomplished in a duration of $1/(4g_{AB}^{10,01})$ [30]. Similarly, we can tune other levels of the qubits into resonance and realize iSWAP operations among other basis states. For the CCZS gate studied here, an iSWAP gate between $|11\rangle$ and $|20\rangle$ would be desired. In order to bring these two states into resonance, we simply tune the qubits until the condition of $f_{21}^{A} = f_{10}^{A} + \alpha_A = f_{10}^{B}$ is satisfied. Under this condition, an energy exchange between $|11\rangle$ and $|20\rangle$ occurs at a rate of $2g_{AB}^{11,20}$, which approximately equals $2\sqrt{2}g_{AB}^{10,01}$ for transmon qubits [31]. Therefore in the subspace of $\{|11\rangle, |20\rangle\}$, the SWAP matrix reads

$$U_{AB}(\theta_{AB}) = \begin{pmatrix} \cos\dfrac{\theta_{AB}}{2} & -\mathrm{i}\sin\dfrac{\theta_{AB}}{2} \\ -\mathrm{i}\sin\dfrac{\theta_{AB}}{2} & \cos\dfrac{\theta_{AB}}{2} \end{pmatrix}, \tag{1}$$

where $\theta_{AB} = 2\sqrt{2}g_{AB}t$ is an effective rotation angle determined by the duration and strength of the coupling. Given the coupling strength of $g_{AB}/(2\pi) = 14.2$ MHz in our sample, an iSWAP gate (i.e., $\theta_{AB} = \pi$) between $|11\rangle$ and $|20\rangle$ is accomplished at a duration of $1/(4\sqrt{2}g_{AB}) \approx$ 12.5 ns.

Next, we define a three-qubit operation of U_F by cascading three iSWAP gates between adjacent qubits as the following:

$$\begin{aligned} U_F &= U_{AB}(\pi)U_{AC}(\pi)U_{AB}(\pi) \\ &= \begin{pmatrix} 1 & 0 & 0 & 0 & 0 & 0 & 0 & 0 \\ 0 & 1 & 0 & 0 & 0 & 0 & 0 & 0 \\ 0 & 0 & 1 & 0 & 0 & 0 & 0 & 0 \\ 0 & 0 & 0 & 1 & 0 & 0 & 0 & 0 \\ 0 & 0 & 0 & 0 & 1 & 0 & 0 & 0 \\ 0 & 0 & 0 & 0 & 0 & 0 & -1 & 0 \\ 0 & 0 & 0 & 0 & 0 & -1 & 0 & 0 \\ 0 & 0 & 0 & 0 & 0 & 0 & 0 & -1 \end{pmatrix}. \end{aligned} \tag{2}$$

The circuit diagram of U_F is shown in Fig. 1(b). Table 1 lists all the intermediate and final outcoming states when applying U_F to different initial states. Only when the control qubit Q_A is in the state $|1\rangle$ are the states of Q_B and Q_C swapped. Therefore U_F is indeed a Fredkin-like CCZS gate [19, 22]. We note that the second excited state of the control-qubit Q_A is used as an auxiliary state that participates in the gate operation but returns to zero population at the end. The overall duration of this gate is around 40 ns, including three iSWAP gates which lasting for 12.5 ns and buffer periods between the iSWAP gates.

Table 1 List of states after each step of the iSWAP gate.

Initial state	After first $U_{AB}(\pi)$	After $U_{AC}(\pi)$	After last $U_{AB}(\pi)$
$\|000\rangle$	$\|000\rangle$	$\|000\rangle$	$\|000\rangle$
$\|001\rangle$	$\|001\rangle$	$\|001\rangle$	$\|001\rangle$
$\|010\rangle$	$\|010\rangle$	$\|010\rangle$	$\|010\rangle$
$\|011\rangle$	$\|011\rangle$	$\|011\rangle$	$\|011\rangle$
$\|100\rangle$	$\|100\rangle$	$\|100\rangle$	$\|100\rangle$
$\|101\rangle$	$\|101\rangle$	$-\mathrm{i}\|200\rangle$	$-\|110\rangle$
$\|110\rangle$	$-\mathrm{i}\|200\rangle$	$-\|101\rangle$	$-\|101\rangle$
$\|111\rangle$	$-\mathrm{i}\|201\rangle$	$-\mathrm{i}\|201\rangle$	$-\|111\rangle$

We experimentally characterize the above Fredkin-like CCZS gate by applying the operation U_F on the eight three-qubit computational basis states, and measuring the corresponding final states. Figure 1(c) is the overall circuit diagram where single-qubit gates for preparing the initial states and for rotating the final states onto proper measurement basis are included. The obtained results are used to construct the truth table of the gate process, shown in Fig. 2. A good agreement is observed between the experimental data and theoretical result represented by Eq. (2). The fidelities of all eight output states are calculated and show a significant dependence on the relevant decoherence times. The truth table fidelity is also calculated as $F = (1/8)\mathrm{Tr}(|U_{\mathrm{exp}}| \cdot |U_{\mathrm{F}}|) =$ 91.2%, where U_{exp} is the measured truth table in Fig. 2. This fidelity evaluates the average performance of the Fredkin-like CCZS gate acting on different initial states [32].

To examine the causes for this relatively low fidelity, we ran a numerical simulation using the parameters of

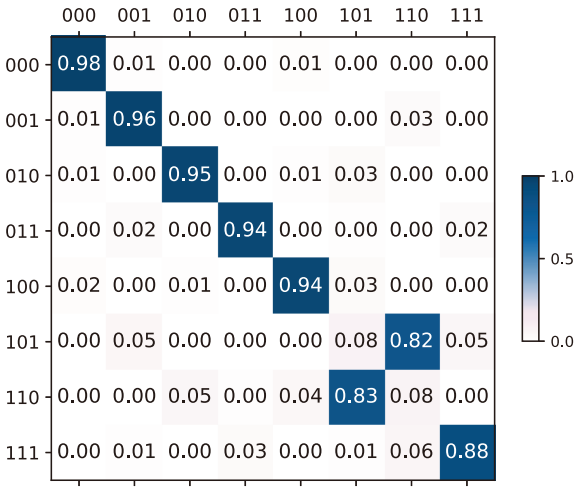

Fig. 2 Measured truth table for our three-qubit CCZS gate. This truth table is to be compared with U_F in Eq. (2). The truth table fidelity is calculated as $F = (1/8)\mathrm{Tr}(|U_{\mathrm{exp}}| \cdot |U_F|) = 91.2\%$.

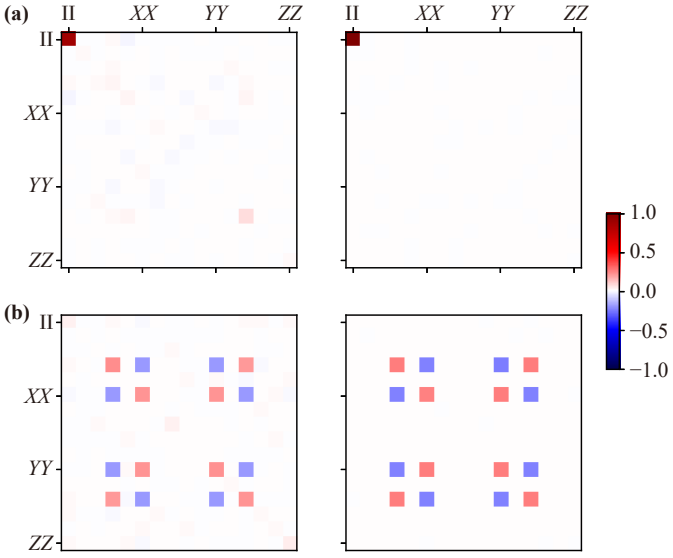

Fig. 3 Experimental (left column) and ideal (right column) quantum process tomography matrices χ_{exp} and χ_{ideal} for the two target qubits. The control qubit Q_A is prepared in **(a)** $|0\rangle$ and **(b)** $|1\rangle$, respectively.

qubits' characterizations (i.e., frequencies, decoherence times, and coupling strength) extracted from experiments and obtained a truth table with a fidelity of nearly 97%, which is limited by qubit dephasing and unwanted transitions such as $|10\rangle \leftrightarrow |01\rangle$. Therefore we conclude that the difference between the experimental results and the simulation mainly comes from the distortion in the square waves transmitted on the z-lines for tuning qubits' frequencies. Such distortion affects the gate operation by inducing an incomplete swap between $|11\rangle$ and $|20\rangle$, which is technically challenging to characterize and is thus not included in our simulation. Moreover, the gate fidelity also depends on the strength of the zz coupling between qubits. When this strength decreases, the experimental fidelity will be significantly improved. The truth table measures the probability distribution of the quantum states and may underestimate phase errors in the corresponding process [32]. To further obtain information about the phase of the unitary, we perform quantum process tomography for the two target qubits Q_B, Q_C when the control qubit Q_A is prepared in $|0\rangle$ or $|1\rangle$ [33]. We prepare 16 two-qubit product states where the state of each qubit is selected from the set $\{|0\rangle, (|0\rangle - \mathrm{i}|1\rangle)/\sqrt{2}, (|0\rangle + |1\rangle)/\sqrt{2}, |1\rangle\}$. Following the two-qubit state tomography, we reconstruct the experimental process matrix χ_{exp}. The experimental and ideal quantum process tomography matrices χ_{exp} and χ_{ideal} are given in Fig. 3 respectively. The process fidelity $\mathrm{Tr}(\chi^0_{\mathrm{exp}}\chi^0_{\mathrm{ideal}}) = 86.0\%$, $\mathrm{Tr}(\chi^1_{\mathrm{exp}}\chi^1_{\mathrm{ideal}}) = 81.1\%$ when the control qubit Q_A is prepared in $|0\rangle$ and $|1\rangle$, respectively.

To demonstrate potential applications of the above Fredkin-like CCZS gate, we use it to generate a maximal entangled three-qubit Greenberger–Horne–Zeilinger (GHZ) state. It is straightforward to verify that when applying U_F of Eq. (2) to an initial product state (i.e., non-entangled) of $\cos(\theta/4)|001\rangle - \sin(\theta/4)|101\rangle$, the ideal final result should be $\cos(\theta/4)|001\rangle + \sin(\theta/4)|110\rangle$. Here θ is set by the single-qubit gate acting upon the control qubit Q_A in the state preparation. At exactly $\theta = \pi$, the above state becomes a GHZ state of $\frac{1}{\sqrt{2}}(|001\rangle + |110\rangle)$. Indeed, Fig. 4(a) plots the populations of $|001\rangle$ and $|110\rangle$ as a function of θ. It is clear that the two states have nearly the same populations at $\theta = \pi$.

To benchmark the fidelity of the generated GHZ state, we perform quantum state tomography (QST) measurement. Because we can only do measurements along the z axis of the transmon qubits, single-qubit rotations of $R_x(\pi/2)$, $R_y(\pi/2)$, and identity gates are applied to map the qubit states to the desired measurement axis for joint readout. Therefore, we need to perform 27 different joint projection measurements of $(\sigma_x\sigma_x\sigma_x, \sigma_x\sigma_x\sigma_y, ..., \sigma_z\sigma_z\sigma_z)$, with each measurement having 8 possible outcomes. The reconstruction of a three-qubit state can then be achieved using the above measured results, following a standard protocol. Figures 4(b) and (c) respectively show one example of the real and imaginary parts of the reconstructed density matrix of the GHZ state generated using our scheme. The fidelity of this GHZ state is calculated to be 96.5%. We further generate the same GHZ state by using the traditional controlled-Z (CZ) gate and single-qubit gates, where the CZ gate is realized by the $|11\rangle \leftrightarrow |20\rangle$ SWAP operation $U(\theta)$ with a rotation angle $\theta = \pi$. Figures 4(d) and (e) respectively show the real and imaginary parts of the reconstructed

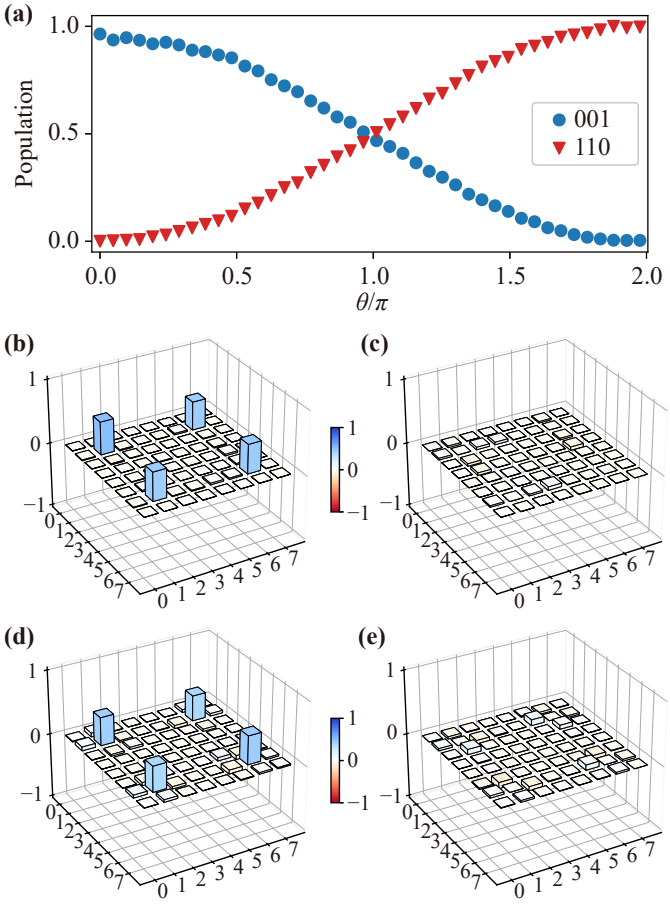

Fig. 4 Generation and benchmarking of a three-qubit GHZ state using our Fredkin-like CCZS gate. **(a)** The measured populations associated with the state of $\cos(\theta/4)|001\rangle - \sin(\theta/4)|110\rangle$ when a CCZS gate is applied to a direct product state of $\cos(\theta/4)|001\rangle - \sin(\theta/4)|101\rangle$. When $\theta = \pi$, the GHZ state $\frac{1}{\sqrt{2}}(|001\rangle + |110\rangle)$ is produced. **(b–e)** The reconstructed density matrix for the GHZ state $\frac{1}{\sqrt{2}}(|001\rangle + |110\rangle)$ using QST. (b) and (c) are real and imaginary parts for the case of applying the CCZS to generate the GHZ state, respectively. (d) and (e) are real and imaginary parts for the case of using traditional CZ gate and single-qubit gates, respectively.

density matrix of the GHZ state generated this way. The fidelity can be calculated to be 91.7%, which is lower than that of the GHZ state generated using our Fredkin-like CCZS gate.

Finally, we note that the above Fredkin-like CCZS gate is of course just a specific member of the family of general CCZS gates. Indeed, in the following we show that a controlled-SWAP operation between the states of Q_B and Q_C with an arbitrary swap angle can be easily realized in our scheme. For this purpose, we simply fix θ_{AB}, the swap angle between Q_A and Q_B, to be π for the first and third iSWAP gates in U_F, and only vary the other swap angle of θ_{AC} for the intermediate iSWAP gate. Therefore we have $U_F = U_{AB}(\pi)U_{AC}(\theta_{AC})U_{AB}(\pi)$. Applying it to an initial state $|110\rangle$, one obtains the

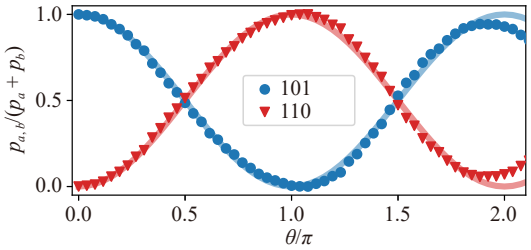

Fig. 5 Demonstration of a controlled three-qubit iSWAP operation with an arbitrary angle. The populations of the $|101\rangle$ state (blue dots) and $|110\rangle$ state (red triangles) are measured as a function of θ_{AC} in $U_F(\theta_{AC}) = U_{AB}(\pi)U_{AC}(\theta_{AC})U_{AB}(\pi)$. When $\theta_{AC} = \pi$, $|101\rangle$ is completely transferred into $|110\rangle$. Lines are a guide to the eye representing the theoretical prediction without decoherence and leakage errors.

following evolution: $|110\rangle \to -i|200\rangle \to -i\cos(\theta_{AC})|200\rangle - \sin(\theta_{AC})|101\rangle \to -\cos(\theta_{AC})|110\rangle - \sin(\theta_{AC})|101\rangle$. Similar analysis can be made for the initial state $|101\rangle$. Therefore we are able to realize a SWAP operation between the states of Q_B and Q_C with an arbitrary angle set by θ_{AC}.

Figure 5 shows the experimental data and numerical simulations of such controlled-SWAP operation with a tunable angle. Here the normalized relative state populations are plotted as a function of the control parameter θ_{AC}. The three-qubit system is first prepared into the initial state of $|101\rangle$, then θ_{AC} is swept from 0 to 2π. During the course, the measured populations of the two states of $|101\rangle$ (blue dots) and $|110\rangle$ (red triangles) are exchanged. At $\theta_{AC} = \pi$, a complete swap between the states of Q_B and Q_C is accomplished. The experimental data agree with the theoretical simulations (lines) reasonably well. The small discrepancy towards the end may result from two factors: decoherence and distortion in the flux line for tuning the frequency of Q_C. Compared to a previous work [22] where the swap angle between the two target qubits relies on both the coupling strengths and frequency detunings, the scheme used here is simpler to implement and also more flexible.

In conclusion, we have experimentally demonstrated a three-qubit CCZS gate using superconducting circuits. Hardware efficiency is achieved by leveraging the higher levels of the transmon qubits for realizing SWAP operations of $|11\rangle \leftrightarrow |20\rangle$ between the control and two target qubits, which is the essential part of our scheme for a general CCZS gate. Compared to other implementations of similar three-qubit gates where only two levels of each qubit are used, our scheme makes a good use of the available resources in the relevant Hilbert space. Since we only use the second excited state of the control qubit as an auxiliary state, it also makes the gate implementation and control much simpler. In addition, the duration of our CCZS gate is only 40 ns, being comparable to that of typical single- and two-qubit gates widely used on superconducting circuits. Therefore our CCZS gate is hardware efficient, straightforward to implement, and of

short duration. These advantages are particularly welcome for potential QIP applications in the NISQ era. As a demonstration, we have used our CCZS gate to generate a GHZ state with a fidelity of 96.5%. Lastly, we want to point out that the scheme can be readily extended for implementing a general controlled-SWAP gate involving n qubits, which provides an alternative option to the existing methods [32].

Declarations The authors declare that they have no competing interests and there are no conflicts.

Acknowledgements This work was supported by the Key-Area Research and Development Program of Guangdong Province (No. 2018B030326001), the National Natural Science Foundation of China (Nos. 12074166 and 12004162), and the Guangdong Provincial Key Laboratory (No. 2019B121203002).

References

1. S. Krinner, N. Lacroix, A. Remm, A. Di Paolo, E. Genois, C. Leroux, C. Hellings, S. Lazar, F. Swiadek, J. Herrmann, G. J. Norris, C. K. Andersen, M. Müller, A. Blais, C. Eichler, and A. Wallraff, Realizing repeated quantum error correction in a distance-three surface code, *Nature* 605(7911), 669 (2022)
2. Y. Zhao, Y. Ye, H. L. Huang, Y. Zhang, D. Wu, H. Guan, Q. Zhu, Z. Wei, T. He, S. Cao, F. Chen, T. H. Chung, H. Deng, D. Fan, M. Gong, C. Guo, S. Guo, L. Han, N. Li, S. Li, Y. Li, F. Liang, J. Lin, H. Qian, H. Rong, H. Su, L. Sun, S. Wang, Y. Wu, Y. Xu, C. Ying, J. Yu, C. Zha, K. Zhang, Y. H. Huo, C. Y. Lu, C. Z. Peng, X. Zhu, and J. W. Pan, Realization of an error-correcting surface code with superconducting qubits, *Phys. Rev. Lett.* 129(3), 030501 (2022)
3. Z. Ni, S. Li, X. Deng, Y. Cai, L. Zhang, W. Wang, Z. B. Yang, H. Yu, F. Yan, S. Liu, C. L. Zou, L. Sun, S. B. Zheng, Y. Xu, and D. Yu, Beating the break-even point with a discrete-variable-encoded logical qubit, *Nature* 616(7955), 56 (2023)
4. J. Preskill, Quantum computing in the NISQ era and beyond, *Quantum* 2, 79 (2018)
5. K. Bharti, A. Cervera-Lierta, T. H. Kyaw, T. Haug, S. Alperin-Lea, A. Anand, M. Degroote, H. Heimonen, J. S. Kottmann, T. Menke, W. K. Mok, S. Sim, L. C. Kwek, and A. Aspuru-Guzik, Noisy intermediate-scale quantum algorithms, *Rev. Mod. Phys.* 94(1), 015004 (2022)
6. B. Cheng, X. H. Deng, X. Gu, Y. He, G. Hu, P. Huang, J. Li, B. C. Lin, D. Lu, Y. Lu, C. Qiu, H. Wang, T. Xin, S. Yu, M. H. Yung, J. Zeng, S. Zhang, Y. Zhong, X. Peng, F. Nori, and D. Yu, Noisy intermediate-scale quantum computers, *Front. Phys.* 18(2), 21308 (2023)
7. A. Peruzzo, J. McClean, P. Shadbolt, M. H. Yung, X. Q. Zhou, P. J. Love, A. Aspuru-Guzik, and J. L. O'Brien, A variational eigenvalue solver on a photonic quantum processor, *Nat. Commun.* 5(1), 4213 (2014)
8. A. Kandala, A. Mezzacapo, K. Temme, M. Takita, M. Brink, J. M. Chow, and J. M. Gambetta, Hardware-efficient variational quantum eigensolver for small molecules and quantum magnets, *Nature* 549(7671), 242 (2017)
9. J. I. Colless, V. V. Ramasesh, D. Dahlen, M. S. Blok, M. E. Kimchi-Schwartz, J. R. McClean, J. Carter, W. A. de Jong, and I. Siddiqi, Computation of molecular spectra on a quantum processor with an error-resilient algorithm, *Phys. Rev. X* 8(1), 011021 (2018)
10. F. Petiziol, M. Sameti, S. Carretta, S. Wimberger, and F. Mintert, Quantum simulation of three-body interactions in weakly driven quantum systems, *Phys. Rev. Lett.* 126(25), 250504 (2021)
11. Z. Wang, Z. Y. Ge, Z. Xiang, X. Song, R. Z. Huang, P. Song, X. Y. Guo, L. Su, K. Xu, D. Zheng, and H. Fan, Observation of emergent $\mathcal{Z}_2$ gauge invariance in a superconducting circuit, *Phys. Rev. Res.* 4(2), L022060 (2022)
12. X. Zhang, W. Jiang, J. Deng, K. Wang, J. Chen, P. Zhang, W. Ren, H. Dong, S. Xu, Y. Gao, F. Jin, X. Zhu, Q. Guo, H. Li, C. Song, A. V. Gorshkov, T. Iadecola, F. Liu, Z. X. Gong, Z. Wang, D. L. Deng, and H. Wang, Digital quantum simulation of floquet symmetry-protected topological phases, *Nature* 607(7919), 468 (2022)
13. M. S. Kang, J. Heo, S. G. Choi, S. Moon, and S. W. Han, Optical Fredkin gate assisted by quantum dot within optical cavity under vacuum noise and sideband leakage, *Sci. Rep.* 10(1), 5123 (2020)
14. D. G. Cory, M. D. Price, W. Maas, E. Knill, R. Laflamme, W. H. Zurek, T. F. Havel, and S. S. Somaroo, Experimental quantum error correction, *Phys. Rev. Lett.* 81(10), 2152 (1998)
15. B. P. Lanyon, M. Barbieri, M. P. Almeida, T. Jennewein, T. C. Ralph, K. J. Resch, G. J. Pryde, J. L. O'Brien, A. Gilchrist, and A. G. White, Simplifying quantum logic using higher-dimensional Hilbert spaces, *Nat. Phys.* 5(2), 134 (2009)
16. T. Monz, K. Kim, W. Hänsel, M. Riebe, A. S. Villar, P. Schindler, M. Chwalla, M. Hennrich, and R. Blatt, Realization of the quantum Toffoli gate with trapped ions, *Phys. Rev. Lett.* 102(4), 040501 (2009)
17. A. Fedorov, L. Steffen, M. Baur, M. P. da Silva, and A. Wallraff, Implementation of a Toffoli gate with superconducting circuits, *Nature* 481(7380), 170 (2012)
18. T. Roy, S. Hazra, S. Kundu, M. Chand, M. P. Patankar, and R. Vijay, Programmable superconducting processor with native three-qubit gates, *Phys. Rev. Appl.* 14(1), 014072 (2020)
19. X. Gu, J. Fernández-Pendás, P. Vikstål, T. Abad, C. Warren, A. Bengtsson, G. Tancredi, V. Shumeiko, J. Bylander, G. Johansson, and A. F. Kockum, Fast multiqubit gates through simultaneous two-qubit gates, *PRX Quantum* 2(4), 040348 (2021)
20. A. J. Baker, G. B. P. Huber, N. J. Glaser, F. Roy, I. Tsitsilin, S. Filipp, and M. J. Hartmann, Single shot i-Toffoli gate in dispersively coupled superconducting qubits, *Appl. Phys. Lett.* 120(5), 054002 (2022)
21. Y. Kim, A. Morvan, L. B. Nguyen, R. K. Naik, C. Junger, L. Chen, J. M. Kreikebaum, D. I. Santiago, and I. Siddiqi, High-fidelity three-qubit i-Toffoli gate for fixed-frequency superconducting qubits, *Nat. Phys.* 18(7), 783 (2022)

22. C. W. Warren, J. Fernández-Pendás, S. Ahmed, T. Abad, A. Bengtsson, J. Biznárová, K. Debnath, X. Gu, C. Križan, A. Osman, A. F. Roudsari, P. Delsing, G. Johansson, A. F. Kockum, G. Tancredi, and J. Bylander, Extensive characterization and implementation of a family of three-qubit gates at the coherence limit, *npj Quantum Inf.* 9, 44 (2023)
23. L. B. Nguyen, Y. Kim, A. Hashim, N. Goss, B. Marinelli, B. Bhandari, D. Das, R. K. Naik, J. M. Kreikebaum, A. N. Jordan, D. I. Santiago, and I. Siddiqi, Programmable Heisenberg interactions between floquet qubits, *Nat. Phys.* 20(2), 240 (2024)
24. R. B. Patel, J. Ho, F. Ferreyrol, T. C. Ralph, and G. J. Pryde, A quantum Fredkin gate, *Sci. Adv.* 2(3), e1501531 (2016)
25. W. Feng and D. Wang, Quantum Fredkin gate based on synthetic three-body interactions in superconducting circuits, *Phys. Rev. A* 101(6), 062312 (2020)
26. P. Maity and M. Purkait, Implementation of a holonomic 3-qubit gate using Rydberg superatoms in a microwave cavity, *Eur. Phys. J. Plus* 137(12), 1299 (2022)
27. Y. Li, L. Wan, H. Zhang, H. Zhu, Y. Shi, L. K. Chin, X. Zhou, L. C. Kwek, and A. Q. Liu, Quantum Fredkin and Toffoli gates on a versatile programmable silicon photonic chip, *npj Quantum Inf.* 8, 112 (2022)
28. J. Koch, T. M. Yu, J. Gambetta, A. A. Houck, D. I. Schuster, J. Majer, A. Blais, M. H. Devoret, S. M. Girvin, and R. J. Schoelkopf, Charge-insensitive qubit design derived from the Cooper pair box, *Phys. Rev. A* 76(4), 042319 (2007)
29. Y. Xu, J. Chu, J. Yuan, J. Qiu, Y. Zhou, L. Zhang, X. Tan, Y. Yu, S. Liu, J. Li, F. Yan, and D. Yu, High-fidelity, high-scalability two-qubit gate scheme for superconducting qubits, *Phys. Rev. Lett.* 125(24), 240503 (2020)
30. C. Song, K. Xu, W. Liu, C. Yang, S. B. Zheng, H. Deng, Q. Xie, K. Huang, Q. Guo, L. Zhang, P. Zhang, D. Xu, D. Zheng, X. Zhu, H. Wang, Y. A. Chen, C. Y. Lu, S. Han, and J. W. Pan, 10-qubit entanglement and parallel logic operations with a superconducting circuit, *Phys. Rev. Lett.* 119(18), 180511 (2017)
31. P. Krantz, M. Kjaergaard, F. Yan, T. P. Orlando, S. Gustavsson, and W. D. Oliver, A quantum engineer's guide to superconducting qubits, *Appl. Phys. Rev.* 6(2), 021318 (2019)
32. J. Chu, X. He, Y. Zhou, J. Yuan, L. Zhang, Q. Guo, Y. Hai, Z. Han, C. K. Hu, W. Huang, H. Jia, D. Jiao, S. Li, Y. Liu, Z. Ni, L. Nie, X. Pan, J. Qiu, W. Wei, W. Nuerbolati, Z. Yang, J. Zhang, Z. Zhang, W. Zou, Y. Chen, X. Deng, X. Deng, L. Hu, J. Li, S. Liu, Y. Lu, J. Niu, D. Tan, Y. Xu, T. Yan, Y. Zhong, F. Yan, X. Sun, and D. Yu, Scalable algorithm simplification using quantum AND logic, *Nat. Phys.* 19(1), 126 (2023)
33. C. K. Hu, J. Yuan, B. A. Veloso, J. Qiu, Y. Zhou, L. Zhang, J. Chu, O. Nurbolat, L. Hu, J. Li, Y. Xu, Y. Zhong, S. Liu, F. Yan, D. Tan, R. Bachelard, A. C. Santos, C. Villas-Boas, and D. Yu, Native conditional iSWAP operation with superconducting artificial atoms, *Phys. Rev. Appl.* 20(3), 034072 (2023)